

**Bio-crude oils production from wheat stem under subcritical water conditions and batch adsorption of post-hydrothermal liquefaction aqueous phase onto activated hydrochars**

Marrakchi, Fatma; Toor, Saqib; Nielsen, Asbjørn Haaning; Pedersen, Thomas Helmer; Rosendahl, Lasse

*Published in:*  
Chemical Engineering Journal

*DOI (link to publication from Publisher):*  
[10.1016/j.cej.2022.139293](https://doi.org/10.1016/j.cej.2022.139293)

*Creative Commons License*  
CC BY 4.0

*Publication date:*  
2023

*Document Version*  
Publisher's PDF, also known as Version of record

[Link to publication from Aalborg University](#)

*Citation for published version (APA):*

Marrakchi, F., Toor, S., Nielsen, A. H., Pedersen, T. H., & Rosendahl, L. (2023). Bio-crude oils production from wheat stem under subcritical water conditions and batch adsorption of post-hydrothermal liquefaction aqueous phase onto activated hydrochars. *Chemical Engineering Journal*, 452, Article 139293. <https://doi.org/10.1016/j.cej.2022.139293>

**General rights**

Copyright and moral rights for the publications made accessible in the public portal are retained by the authors and/or other copyright owners and it is a condition of accessing publications that users recognise and abide by the legal requirements associated with these rights.

- Users may download and print one copy of any publication from the public portal for the purpose of private study or research.
- You may not further distribute the material or use it for any profit-making activity or commercial gain
- You may freely distribute the URL identifying the publication in the public portal -

**Take down policy**

If you believe that this document breaches copyright please contact us at [vbn@aub.aau.dk](mailto:vbn@aub.aau.dk) providing details, and we will remove access to the work immediately and investigate your claim.

Downloaded from [vbn.aau.dk](http://vbn.aau.dk) on: December 05, 2025



# Bio-crude oils production from wheat stem under subcritical water conditions and batch adsorption of post-hydrothermal liquefaction aqueous phase onto activated hydrochars

Fatma Marrakchi<sup>a,\*</sup>, Saqib Sohail Toor<sup>a</sup>, Asbjørn Haaning Nielsen<sup>b</sup>, Thomas Helmer Pedersen<sup>a</sup>, Lasse Aistrup Rosendahl<sup>a</sup>

<sup>a</sup> AAU Energy, Aalborg University, Pontoppidanstræde 111, 9220 Aalborg, Denmark

<sup>b</sup> AAU Build, Aalborg University, Thomas Manns Vej 23, 9220 Aalborg, Denmark

## ARTICLE INFO

### Keywords:

Hydrothermal liquefaction  
Biocrude  
Hydrochar  
Activation  
Aqueous phase  
Batch adsorption

## ABSTRACT

Hydrothermal liquefaction (HTL) is known to be a promising technology to produce crude bio-oils as intermediate to drop-in transport fuels. However, the co-production of liquefaction wastewater (HTL-AP) and hydrochar residues (HCs) limits the economic viability and technical scalability. Hence, the objective of this work is to study the effect of catalysts NaOH, KOH, Na<sub>2</sub>CO<sub>3</sub>, K<sub>2</sub>CO<sub>3</sub>, H<sub>3</sub>PO<sub>4</sub>, FeCl<sub>3</sub> and Fe<sub>2</sub>O<sub>3</sub> in the HTL reaction medium and on the characteristics of derived crude bio-oils from wheat stem under subcritical conditions at 350 °C for 15 min. Likewise, the mentioned chemical agents were used to enhance the structural, morphological, and chemical surface properties of the HCs for the uptake of the organic adsorbates and nutrients from the HTL-AP. A yield of 30.85 wt% crude bio-oil, having the highest HHV of 34.36 MJ/kg, and lowest 22.03 wt% hydrochar are achieved under Na<sub>2</sub>CO<sub>3</sub>-catalyzed HTL. In contrast, the acidic and Fe-based catalysts revealed a lesser bio-oil yield because of the low pH, which promotes dehydration and polymerization reactions. Reduced Na, K, Fe, and S contents were found in H<sub>3</sub>PO<sub>4</sub>, FeCl<sub>3</sub>, and Fe<sub>2</sub>O<sub>3</sub>-catalyzed biocrudes. This result supports the hypothesis of the *in situ* demetallation during HTL reaction due to their adsorption onto the mesoporous hydrochars with D<sub>p</sub> = 13.77–33.58 nm. The removal efficiency levels for COD, TOC, phenols, total N, P, and dissolved K are 66.67–92.77 %, 62.58–91.84 %, 65.59–99.91 %, 37.63–80.80 %, 96.67–99.90 %, and 45.57–92.36 %, respectively after HTAL-AP treatment. The results demonstrate new insights and directions for the use of activated hydrochar as a low-cost adsorbent for HTL-AP remediation purposes.

## 1. Introduction

With the static global growth of the biomass-derived fuel supply chain, coupled with their inclusion in the long-term decarbonization of many transport enterprises, the sector still addresses the following questions: are the emerging technologies assess the sustainability and scalability of biofuels? and if so, what are the challenges in the implementation of the future global energy–water–climate nexus? [1]. Hydrothermal liquefaction (HTL), which is also known as hydrous pyrolysis, is a thermochemical and emerging technology focusing on the increase of biocrude productivity by reducing the operating temperature (280 °C–400 °C), minimizing energy consumption, and excluding prior drying cost with the exploitation of various high water-containing feedstocks [2]. HTL is a water-driven depolymerization process

performed under closed O<sub>2</sub>-free and sub-critical, near-critical, or supercritical conditions (10–35 MPa), where pressurized hot water serves as a reactant and catalyst that decomposes the biopolymeric structure into co-products, such as liquid, gas, and solid phases [3]. Compared with fast pyrolysis oil, HTL crude bio-oil is typically more stable, and it exhibits lower oxygen and moisture contents with elevated energy density and calorific value (32–44 MJ/kg) [4]. Nonetheless, upgrading via hydrotreatment is required for drop-in transportation-grade fuel. Gaseous products of HTL are primarily composed of CO<sub>2</sub> > 80 % and a small fraction of CO, H<sub>2</sub>, CH<sub>4</sub>, C<sub>2</sub>H<sub>6</sub>, C<sub>2</sub>H<sub>4</sub>, benzene, toluene, and styrene. Compounds such as ethene have been classified as hazardous air pollutants by USEPA; however, they are exempt from the regulation because of their low concentration levels and “net-zero” carbon accountability [1].

\* Corresponding author.

E-mail address: [fmarr@energy.aau.dk](mailto:fmarr@energy.aau.dk) (F. Marrakchi).

<https://doi.org/10.1016/j.cej.2022.139293>

Received 23 June 2022; Received in revised form 10 September 2022; Accepted 14 September 2022

Available online 26 September 2022

1385-8947/© 2022 The Author(s). Published by Elsevier B.V. This is an open access article under the CC BY license (<http://creativecommons.org/licenses/by/4.0/>).

Despite being a competitive technology and apart from crude bio-oil as the target product, the major challenge limiting the economic viability and technical scalability of the HTL-related process is the safe disposal of generated by-products, including nearly 25 wt% to 50 wt% post-hydrothermal aqueous phase (HTL-AP) and 5 wt% to 20 wt% solid hydrochar residues (HCs) [5]. The HTL-AP typically comprises low-molecular-weight acid compounds derived from lignocellulose biomass, reaching acidic pH ranging from 3.5 to 5. A high concentration of organics, ammonia, and organic nitrogen has also been found and confirmed by 46–401 g/L of chemical oxygen demand (COD) and 0.8–7.07 g/L of total nitrogen (TN) [6]. Furthermore, metals, including phosphorus (P), potassium (K), sodium (Na), magnesium (Mg), aluminum (Al), calcium (Ca), and iron (Fe), were observed in the HTL-AP [7]. The discharge of the aqueous HTL directly into the ecosystem without proper treatment is hectic, which would lead to wastewater generation and wastage of environmental resources, nutrient runoff, and eutrophication. The literature has revealed that HTL-AP purification has stringent requirements, as most treatment methods may not accommodate high organic loadings. For example, COD values < 10 g/L are typically required for the processability anaerobic fermentation and bioelectrochemical systems [8]. This strategy suggests that heavy dilutions of HTL-AP, around 100 times, are compelling and challenging, which is economically unfeasible because it involves the usage of freshwater.

Integrating adsorbents such as commercially activated carbons and zeolites can be a potential step to the removal of xenobiotic and recalcitrant organic and nutrient compounds from HTL-AP. However, these expensive adsorbents require a substitute for adsorption sustainability [9]. Solid HCs, which are generated from HTL with carbon as the major element, can be used as low-cost adsorbents. However, its porosity of 0.058–0.082 cm<sup>3</sup>/g and BET specific surface area of 1.56–17 m<sup>2</sup>/g remain comparatively low because of the formation and condensation of hydrocarbons on the surface, thereby clogging pores and reducing its adsorption capacity [10,11]. Activation, in which HCs are impregnated with certain dehydrating agents acting as oxidants (e.g., NaOH, KOH, Na<sub>2</sub>CO<sub>3</sub>, K<sub>2</sub>CO<sub>3</sub>, H<sub>3</sub>PO<sub>4</sub>, and other acid salts) and pyrolyzed under inert atmosphere at 800 °C, could aromatize the HC carbon skeleton, with oxygen-containing functional groups and more developed porous structure with high stability. To the best of our knowledge, existing HTL studies have well-characterized crude bio-oils but have not focused on hydrochar except for primary details such as yield and ultimate analysis. Furthermore, the use of HTL hydrochar as an alternative low cost for commercial adsorbents and wastewater remediation purposes is very less explored in comparison to pyrolytic char. Hence, this research work aimed to study the twofold effect of NaOH, KOH, Na<sub>2</sub>CO<sub>3</sub>, K<sub>2</sub>CO<sub>3</sub>, H<sub>3</sub>PO<sub>4</sub>, FeCl<sub>3</sub>, and Fe<sub>2</sub>O<sub>3</sub> as catalysts in the HTL reaction medium and as dehydrating agents for the enhancement of surface structure, morphology, and chemistry of HTL hydrochar. Besides, the adsorptive properties of the prepared activated hydrochars for the uptake and recovery of organics (COD, TOC, phenols) and nutrients (TN, TP, and dissolved K) from the HTL aqueous solution were tested.

## 2. Materials and methods

### 2.1. Wheat stem, chemicals, and experimental activities

Wheat stem (WS), which dominated the production in the EU crop-land by 72 %, or 57 million ha, in 2019 [12], was collected from the cultivation field in Aalborg, Denmark, after harvesting grains. WS was ground and sieved to obtain particles with a size of < 250 µm. Stem, which is used as a starting material, contained 6 % moisture (Kern Moisture Analyzer MLS at 105 °C), 7 % ash (ASTM D4852 standard) [13], 73.65 % volatile matter and 13.62 % fixed carbon (ARES-G2, TA Instrument, Heating rate of 10 °C/min from 100 to 900 °C with a N<sub>2</sub> purge rate of 20 mL/min). WS' biochemical composition was characterized in a previous study by fiber method (FOSS Cyclotec 1093) and

contains 37.92 % cellulose, 30.24 % hemicellulose, 4.69 % lignin [14]. Sodium hydroxide (NaOH, >99 %), potassium hydroxide (KOH, >99 %), sodium carbonate (Na<sub>2</sub>CO<sub>3</sub>), potassium carbonate (K<sub>2</sub>CO<sub>3</sub>, 99.99 %), phosphoric acid (H<sub>3</sub>PO<sub>4</sub>, 85 %), ferric chloride (FeCl<sub>3</sub>, >99 %), ferric oxide (Fe<sub>2</sub>O<sub>3</sub>, >99 %), acetone (C<sub>3</sub>H<sub>6</sub>O, ≥ 99.5 %), and diethyl ether (C<sub>4</sub>H<sub>10</sub>O, ≥99.5 %) were purchased from VWR Company, Denmark. A summary of the experimental activities followed in this investigation starting from HTL of WS, preparation of activated HC adsorbents, and adsorption study of organic adsorbates and nutrients from HTL-AP was illustrated in the flowchart (Fig. 1).

### 2.2. Hydrothermal liquefaction of WS and analysis of crude bio-oils and gases

A high-pressure stainless steel autoclave reactor with a volumetric capacity of 0.4 L and maximum operating limits of 500 °C and 35 MPa was used for the HTL of WS. Initially, 50 g of WS was mixed with different catalysts, including X = NaOH, KOH, Na<sub>2</sub>CO<sub>3</sub>, K<sub>2</sub>CO<sub>3</sub>, H<sub>3</sub>PO<sub>4</sub>, FeCl<sub>3</sub>, and Fe<sub>2</sub>O<sub>3</sub>, at a fixed weight ratio percentage of 2% =  $\frac{W_X}{W_{WS}} \times 100$  in 0.2 L of distilled water. The reactor was pressurized with 2 MPa of nitrogen gas to create an anoxic inert atmosphere condition. Then, the mixture was stirred at a constant stirring speed of 400 rpm to ensure complete homogenization prior to the HTL reaction. The temperature was increased from room temperature to 350 °C at a rate of 10 °C/min and maintained for 15 min [15,16]. The autogenous pressure generated during the reaction was in the range of 22–25 MPa. The liquefaction products at different catalysts (X) were labeled as “Gas@X”, “AP@X”, “Oil@X”, and “HC@X”, consisting of gases (e.g., CO, CO<sub>2</sub>, CH<sub>4</sub>, and H<sub>2</sub>), aqueous phase, crude bio-oil, and hydrochar, respectively.

A non-condensable sample, namely, Gas@X, was collected after the reaction system was cooled in a stainless-steel gas sampling bomb, and the leftover gases were vented out. Gas@X was analyzed via GC using a Shimadzu Inc. GC-2010 system equipped with a GC-BID detector and Supelco 1006 PLOT column. The composition of the gas was evaluated by comparing its retention time with the mass spectral data of an authentic standard gas. The obtained extracted liquefaction products with acetone were collected and double filtered to separate HC@X and liquid products (AP@X and Oil@X). Thereafter, the acetone was removed using a vacuum rotary evaporator at 60 °C and 50 KPa. Then, the oil phase was separated from the aqueous phase by using a diethyl ether solvent. The Oil@X yield derived from the HTL of WS under subcritical water conditions at different catalysts (X) was calculated on a dry-ash-free (daf) basis, following Eq. (1):

$$\text{Oil@X yield (\%)} = \frac{W_{\text{Oil@X}}}{W_{\text{WS,daf}}} \times 100 \quad (1)$$

Ultimate analysis, inorganic fraction, heating values (HHV), and energy recovery (ER) of the obtained Oil@X were determined using a CHN analyzer (PerkinElmer 2400 Series II, ASTM D5291), Inductively Coupled Plasma Atomic Emission Spectroscopy (ICP-AES), oxygen bomb calorimeter (IKA, C2000), and Eq. (2), respectively.

$$\text{ER(\%)} = \frac{\text{HHV}_{\text{Oil@X}}}{\text{HHV}_{\text{WS}}} \times \text{Yield}_{\text{Oil@X}} \quad (2)$$

Furthermore, compositional analyses were performed through TRACE™ 1300 Serie gas chromatography coupled with the ISQ-ID mass spectrometry system (GC–MS). During GC–MS analysis, the Oil@X vapor was separated into several compounds through a CP-9036 capillary column with a dimension of 30 m × 300 µm installed in the GC system. A GC injection port temperature of 300 °C and a split ratio of 20 were maintained using an in-built GC program. The program started at 35 °C with a holding time of 2 min, ramped to 120 °C and maintained for 5 min, then increased to 300 °C and set for 4 min under a steady flow of 1 mL/min of helium as a carrier gas. The chemical constituents of Oil@X were identified and measured with regard to spectrum peaks by

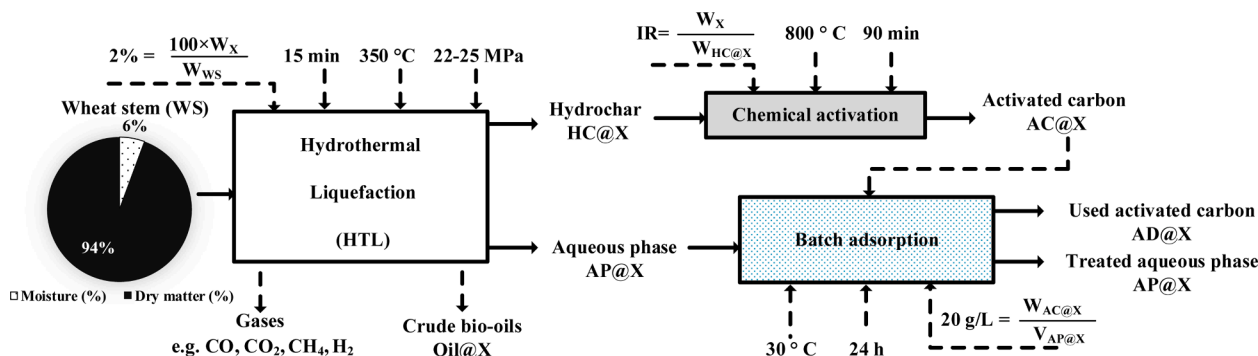


Fig. 1. Schematic description of WS liquefaction under subcritical water conditions without/with catalytic effect ( $X = \text{NaOH}, \text{KOH}, \text{Na}_2\text{CO}_3, \text{K}_2\text{CO}_3, \text{H}_3\text{PO}_4, \text{FeCl}_3, \text{Fe}_2\text{O}_3$ ), preparation of activated HC adsorbents, and post-treatment of HTL aqueous phase.

matching their retention time and the standard mass spectrum library of the National Institute of Standards and Technology installed in a PC database system. The boiling point distribution and their respective fractional cuts composition of the obtained Oil@X was performed according to ASTM D7169-20 standard [17] via simulated-distillation, using a zebron ZB-1XT column  $\times$  (Phenomenex) equipped gas chromatography–flame ionization detector (GC-FID) (Shimadzu, Kyoto, Japan).

### 2.3. Preparation and characterization of activated HCs

HC@X was washed with acetone repeatedly to remove any remaining crude oil, and then yields were calculated after drying at 105 °C (Eq. (3)).

$$\text{HC@X yield (\%)} = \frac{W_{\text{HC@X}}}{W_{\text{WS,dry}}} \times 100 \quad (3)$$

The ACs were subsequently prepared by impregnation of each wheat stem-derived HC using activating agents similar to the defined catalysts in the HTL step (Fig. 1) at an impregnation ratio (IR) of 2 g/g, expressed as the dry weight of X (g) to HC@X (g). For example, the activated HC (AC@NaOH) was prepared from HC@NaOH, resulting from the subcritical catalytic liquefaction of WS with sodium hydroxide. Then, the resulting impregnated HC samples were placed in a stainless-steel tubular reactor, heated up to an activation temperature of 800 °C at a rate of 10 °C/min, and held at this temperature for 90 min [9,18–20]. Nitrogen gas was purged to remove the air in the reactor before and during the process at a flow rate of 100 mL/min and after activation to cool down the samples. The resulting AC@X was rinsed repeatedly with warm distilled water until the filtrate pH reached approximately 6.0–7.0 and dried at 105 °C, and yields were calculated using Eq. (4).

$$\text{AC@X yield (\%)} = \frac{W_{\text{AC@X}}}{W_{\text{HC@X}}} \times \text{HC@X yield (\%)} \quad (4)$$

Surface structure characteristics and morphologies of WS, HC@X, and AC@X were investigated using a Micromeritics ASAP 2460 instrument and a Zeiss Sigma 300 SEM microscope. Specific surface area ( $S_{\text{BET}}$ ,  $\text{m}^2/\text{g}$ ), external surface area ( $S_{\text{ext}}$ ,  $\text{m}^2/\text{g}$ ), micropore surface area ( $S_{\text{micro}}$ ,  $\text{m}^2/\text{g}$ ), mesopore surface area ( $S_{\text{meso}}$ ,  $\text{m}^2/\text{g}$ ), micropore volume ( $V_{\text{micro}}$ ,  $\text{cm}^3/\text{g}$ ), mesopore volume ( $V_{\text{meso}}$ ,  $\text{cm}^3/\text{g}$ ), total pore volume ( $V_{\text{T}}$ ,  $\text{cm}^3/\text{g}$ ), and mean pore diameter ( $D_p$ , nm) were measured using  $\text{N}_2$  adsorption/desorption isotherm at  $-196^\circ\text{C}$ . Furthermore, FTIR spectra of WS, HC@X, AC@X, and AD@X were obtained by using a Perkin Elmer Spectrum GX Infrared Spectrometer from 4000 to  $400\text{ cm}^{-1}$ . Elemental analysis of nutrients (N, P, K) before and after adsorption was performed by FE-SEM Zeiss Sigma 300 coupled with EDX.

### 2.4. Batch adsorption study and HTL aqueous-phase analysis before and after treatment

Prior to adsorption experiments, the clumping of fines present in HTL aqueous phases (AP@X) into larger clusters was conducted for easy physical separation rather than the original particles. The initial pH of each AP@X was adjusted by increasing pH from 10 to 12 using 1 M NaOH solution. Then, polyaluminum chloride (10 wt%) was added and continuously stirred at a dose defined by reaching the pH of 7–8, resulting in the formation of aggregates separated afterward by centrifugation. All the adsorption runs were performed in a batch process using a thermostatic water bath shaker fixed at 150 rpm. An amount of 1 g of each prepared AC@X adsorbent (AC@NaOH, AC@KOH, AC@Na<sub>2</sub>CO<sub>3</sub>, AC@K<sub>2</sub>CO<sub>3</sub>, AC@H<sub>3</sub>PO<sub>4</sub>, AC@FeCl<sub>3</sub>, and AC@Fe<sub>2</sub>O<sub>3</sub>) was added to 50 mL of the collected AP@X (AP@NaOH, AP@KOH, AP@Na<sub>2</sub>CO<sub>3</sub>, AP@K<sub>2</sub>CO<sub>3</sub>, AP@H<sub>3</sub>PO<sub>4</sub>, AP@FeCl<sub>3</sub>, and AP@Fe<sub>2</sub>O<sub>3</sub>), and the mixture was stirred at 30 °C overnight to ensure that adsorption had reached equilibrium.

The initial concentration ( $C_i$ , mg/L) and residual ones ( $C_r$ , mg/L) after purification of COD, total organic carbon (TOC), phenols, TN, total dissolved potassium (K), and total phosphorous (TP) in AP@X solutions were spectrophotometrically measured using the corresponding LCK cuvette tests placed inside the analysis chamber of a UV–Visible colorimeter (Hach Lange, DR 3900) at a maximum wavelength of 314 nm (LCK 314), 435 nm (LCK 386), 510 nm (LCK 346), 345 nm (LCK 138), 695 nm (LCK328), and 880 nm (LCK349), respectively. After adsorption, removal percentages of adsorbates were calculated using Eq. (5), and AD@X (used AC@X) was separated, rinsed with distilled water, and dried. Then, their FTIR spectra were recorded and compared with raw AC@X to understand the adsorption mechanism.

$$\text{Removal (\%)} = \frac{C_i - C_r}{C_i} \times 100 \quad (5)$$

## 3. Results and discussion

### 3.1. Yield and characterization of crude bio-oils

Fig. 2 shows the effects of eight catalysts (X) on the distribution of HTL products via WS conversion at 350 °C for 15 min as the reaction time under subcritical water conditions without and with 2 wt% loading of X with regard to the dried WS mass. As illustrated in Fig. 2, the obtained crude bio-oil (Oil@X) yields were presented as follows: Na<sub>2</sub>CO<sub>3</sub> (30.85 wt%) > NaOH (30.52 wt%) > K<sub>2</sub>CO<sub>3</sub> (28.79 wt%) > KOH (26.57 wt%) > H<sub>2</sub>O (16.35 wt%) > Fe<sub>2</sub>O<sub>3</sub> (14.63 wt%) > FeCl<sub>3</sub> (9.58 wt%) > H<sub>3</sub>PO<sub>4</sub> (8.38 wt%). Among the tested catalysts, alkaline catalysts (Na<sub>2</sub>CO<sub>3</sub> and NaOH followed by K<sub>2</sub>CO<sub>3</sub> and KOH) showed superior catalytic effects in the enhancement of crude bio-oil yields. This result was attributed to the alkalinity of the reaction medium that remarkably affects the HTL pathway by promoting the hydrolytic depolymerization



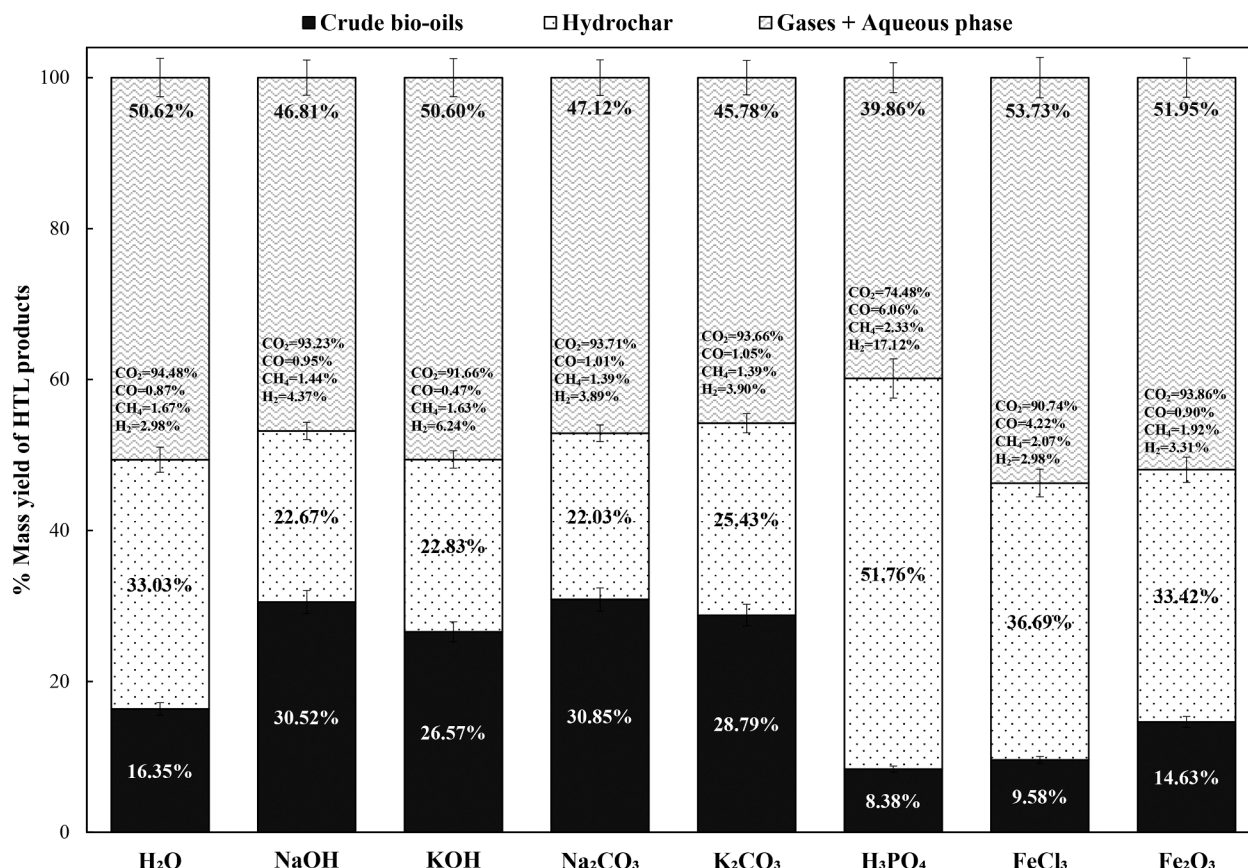


Fig. 2. Effect of different catalysts (X) on the HTL products distribution without/with 2 wt% loading of X with respect to the dried mass of WS at subcritical water conditions (temperature = 350 °C, residence time = 15 min, reaction pressure = 22–25 MPa, and X = NaOH, KOH, Na<sub>2</sub>CO<sub>3</sub>, K<sub>2</sub>CO<sub>3</sub>, H<sub>3</sub>PO<sub>4</sub>, FeCl<sub>3</sub>, Fe<sub>2</sub>O<sub>3</sub>).

of biomacromolecules, such as cellulose, hemicellulose, and lignin, into linear and monocyclic small structures and inhibiting the dehydration and repolymerization of reaction intermediates through the neutralization of carboxylic acids [21,22]. Thus, this reaction dramatically improves the bio-oil yields and reduces HC formation to 22.67 % for HC@NaOH, 22.83 % for HC@KOH, 22.03 % for HC@Na<sub>2</sub>CO<sub>3</sub>, and 25.43 % for HC@K<sub>2</sub>CO<sub>3</sub> compared with non-catalytic HTL experiments (HC@H<sub>2</sub>O, 33.03 %). Furthermore, the yield of Oil@Na<sub>2</sub>CO<sub>3</sub> and Oil@K<sub>2</sub>CO<sub>3</sub> was slightly higher than that of Oil@NaOH and Oil@KOH, indicating the efficiency of alkaline carbonate salts compared with hydroxides. These results were similar to those in the literature because of the generation of secondary promoters of hydroxides and bicarbonates from carbonate salts and water during WS liquefaction [15,23]. Relative to alkaline catalysts, the application of H<sub>3</sub>PO<sub>4</sub> and FeCl<sub>3</sub> increased HC yield to 51.76 % and 36.69 %, which adversely contributed to bio-oil yield reduction to 8.38 % and 9.58 %, respectively. This result may be due to the partial carbonization of organic compounds in Oil@H<sub>3</sub>PO<sub>4</sub> and Oil@FeCl<sub>3</sub> or the formation of viscous liquid intermediates in a low pH medium favoring dehydration, cross-linking, and poly-condensation of secondary reactions and then contributing to the occurrence of char chunks [11]. Correspondingly, Zhou *et al.* [24] found that the presence of sulfuric acid or acetic acid was not effective in achieving optimized bio-oil yield and increasing aqueous phase and char yields. In an acidic environment, decarboxylation and dehydration reactions are apparent for O and H removal, and the gases (Gas@ H<sub>3</sub>PO<sub>4</sub>) are released as carbon oxides (6.06 % CO), light hydrocarbon gases as methane (2.33 % CH<sub>4</sub>), and hydrogen (17.12 % H<sub>2</sub>) liberated as molecular hydrogen and by secondary methane formation [25,26]. For the hematite catalyst, Fe<sub>2</sub>O<sub>3</sub>, no effect on the distribution of HTL products was observed. The yield of Oil@ Fe<sub>2</sub>O<sub>3</sub> (14.63 %), HC@Fe<sub>2</sub>O<sub>3</sub> (35.70 %), and combined AP@ Fe<sub>2</sub>O<sub>3</sub> + Gas@ Fe<sub>2</sub>O<sub>3</sub> (49.67 %) did not differ from the values obtained

at the same operating conditions without a catalyst, including 16.35 % for Oil@H<sub>2</sub>O, 33.03 % for HC@H<sub>2</sub>O, and % 50.62 % for AP@H<sub>2</sub>O + Gas@ H<sub>2</sub>O. Therefore, Fe<sub>2</sub>O<sub>3</sub> had no catalytic activity in promoting crude bio-oil production during WS liquefaction because of its maximum oxidation state (+3). This result was consistent with previous HTL works on oak wood and pinewood sawdust biomasses [22,27].

Crude bio-oil yield is a crucial criterion from an economical point of view and the evaluation of its quality within the application of different catalysts is also important. The elemental composition (%), H/C and O/C ratio, heating values (MJ/kg), and ER (%) of crude bio-oils obtained at 350 °C for 15 min with/without catalysts are summarized in Table 1. Catalytic HTL aimed to decrease the O/C ratio of bio-oil relative to the non-catalytic one; however, the O/C ratio of Oil@H<sub>3</sub>PO<sub>4</sub> was significantly higher than that of Oil@H<sub>2</sub>O. Compared with the WS (%C = 42.15 ± 0.07, %H = 6.15 ± 0.07, %O = 51.45 ± 0.156, %N = 0.25 ± 0.014; O/C = 0.92 ± 0.004; H/C = 1.75 ± 0.017; HHV = 16.69 MJ/kg), the C and H contents of crude bio-oils were considerably higher, whereas the O content evidently declined, leading to higher HHVs of 33.233–34.36 MJ/kg for bio-oils. As shown in Table 1, H/C > 1.232, O/C < 0.168 contents, and HHVs > 32.94 MJ/kg were obtained with the addition of alkaline catalysts compared with the non-catalytic run Oil@H<sub>2</sub>O, leading to higher ER of 53.39 %–62.08 %. This result indicates that deoxygenation reactions were more enhanced in the decarboxylation pathway than in the decarbonylation pathway in the presence of alkali catalysts, leading to the formation of CO<sub>2</sub> (%) > CO (%) during HTL (Fig. 2) [15]. Despite non-variant yields of Oil@FeCl<sub>3</sub> and Oil@Fe<sub>2</sub>O<sub>3</sub> compared with Oil@H<sub>2</sub>O, elemental compositions (C<sub>Oil@FeCl<sub>3</sub></sub> = 75.46%, C<sub>Fe<sub>2</sub>O<sub>3</sub></sub> = 75.55%, O<sub>Oil@FeCl<sub>3</sub></sub> = 14.93%, O<sub>Oil@Fe<sub>2</sub>O<sub>3</sub></sub> = 15.04%) and heating values (HHV<sub>Oil@FeCl<sub>3</sub></sub> = 33.336 MJ/kg, HHV<sub>Fe<sub>2</sub>O<sub>3</sub></sub> = 33.385 MJ/kg) showed comparable results to crude bio-oils obtained via catalytic HTL with alkaline carbonate

**Table 1**

Organic and inorganic composition (%), H/C and O/C ratios, HHV (MJ/kg), and ER (%) of the obtained crude bio-oils at subcritical water condition without/with catalyst.

Crude bio-oils	Ultimate analysis				Atomic ratio		Heavy metals <sup>b</sup> (%)								HHV (MJ/kg)	ER (%)
	C (%)	H (%)	N (%)	O <sup>a</sup> (%)	H/C	O/C	Na	Ca	P	K	Mg	Fe	S			
Oil@H <sub>2</sub> O	74.74	7.67	0.90	16.70	1.232	0.168	0.11	0.09	0.09	0.61	0.02	0.18	3.68	32.94	32.27	
	±0.02	±0.11	±0.02	±0.07	±0.02	±0.00										
Oil@NaOH	75.15	7.88	0.88	16.07	1.258	0.161	0.52	0.02	0.00	0.60	0.00	0.05	0.85	33.23	60.79	
	±1.31	±0.20	±0.46	±1.97	±0.01	±0.02										
Oil@KOH	74.85	7.62	0.82	16.72	1.222	0.167	0.12	0.14	0.02	1.20	0.01	0.23	4.86	33.53	53.39	
	±0.04	±0.04	±0.01	±0.01	±0.00	±0.00										
Oil@Na <sub>2</sub> CO <sub>3</sub>	75.21	7.97	1.66	15.16	1.272	0.151	0.53	0.08	0.02	0.57	0.01	0.28	3.79	33.58	62.08	
	±0.40	±0.06	±0.03	±0.38	±0.02	±0.01										
Oil@K <sub>2</sub> CO <sub>3</sub>	75.65	8.06	1.46	14.84	1.278	0.147	0.09	0.09	0.09	0.75	0.03	0.38	7.74	34.36	59.27	
	±0.27	±0.07	±0.10	±0.01	±0.02	±0.00										
Oil@H <sub>3</sub> PO <sub>4</sub>	67.89	7.42	0.82	23.88	1.311	0.264	0.00	0.00	0.03	0.01	0.00	0.01	0.22	29.99	15.06	
	±0.20	±0.00	±0.10	±0.28	±0.05	±0.00										
Oil@FeCl <sub>3</sub>	75.55	7.98	1.44	15.04	1.268	0.149	0.00	0.01	0.02	0.01	0.00	0.11	0.05	33.34	19.15	
	±0.58	±0.03	±0.04	±0.57	±0.01	±0.01										
Oil@Fe <sub>2</sub> O <sub>3</sub>	75.46	7.83	1.79	14.93	1.245	0.148	0.00	0.01	0.01	0.03	0.00	0.06	0.19	33.39	29.27	
	±0.32	±0.06	±0.03	±0.29	±0.01	±0.00										

<sup>a</sup> : Oxygen contents of Oil@X were calculated by difference O%=100 %-(C + H + N).

<sup>b</sup> : The percentage of each inorganic = (concentration of metal (in mg/kg) × ash mass in Oil@X) × 100/ total concentration of metals (in mg/kg). Ash in Oil@X is determined via TGA analysis (TA Instrument, Discovery SDT 650) by heating to 900 °C and held isothermally for 10 min in an oxygen atmosphere with a purge rate of 20 mL/min.

salts. These results indicate that Fe-based catalysts can promote crude bio-oil quality with minor yield improvement.

The removal of heteroatoms and heavy metals improves crude bio-oil quality, which contributes to less undesirable emissions of NO<sub>x</sub> and SO<sub>x</sub> and increases catalyst lifetime by reducing metal deposition and then catalyst deactivation during upgrading [28]. Table 1 presents the effect of the eight catalysts on Na, Ca, P, K, Mg, Fe, and S concentrations in HTL bio-oils. Only minor quantities of inorganics are detected in crude bio-oils, whereas Ca, P, Mg, and Fe are principally concentrated in HCs after HTL (with weight percentages above 90 %) (Illustration is not shown where the amount of each inorganic element recovered in each product phase was calculated by multiplying the concentration of an element in a phase (mg/kg) by the mass of that phase. The corresponding weight percent was calculated normalizing the total to 100). In addition, K and Na are primarily recovered in the aqueous phase (around 70 wt% in most HTL runs). The similar distribution of inorganic elements after subcritical HTL of animal waste feedstocks was consistent with the present research [29]. Notably, acid and Fe-based catalysts effectively reduced the content of Na, Ca, K, Fe, and S in biocrudes relative to Oil@H<sub>2</sub>O and/or HTL with alkaline catalysts. This outcome may support the hypothesis that their adsorption onto HC@H<sub>3</sub>PO<sub>4</sub>, HC@FeCl<sub>3</sub>, and HC@Fe<sub>2</sub>O<sub>3</sub> contributes to the *in situ* demetallation and reduction of heavy metal contents in Oil@H<sub>3</sub>PO<sub>4</sub>, Oil@FeCl<sub>3</sub>, and Oil@Fe<sub>2</sub>O<sub>3</sub> during their production, respectively.

The functionality of organic compounds presents in non-catalytic and catalytic crude bio-oils, such as Oil@H<sub>2</sub>O, Oil@NaOH, Oil@KOH, Oil@Na<sub>2</sub>CO<sub>3</sub>, Oil@K<sub>2</sub>CO<sub>3</sub>, Oil@H<sub>3</sub>PO<sub>4</sub>, Oil@ FeCl<sub>3</sub>, and Oil@ Fe<sub>2</sub>O<sub>3</sub>, was also categorized by GC–MS and compared (Fig. 3 (a)). The relative concentration of aldehydes, ketones, alcohols, ethers, carboxylic acids, esters, furans, aliphatic and aromatic hydrocarbons, and N-compounds was determined on the basis of the peak area. Low levels of N-containing compounds were observed on crude bio-oils obtained via catalytic HTL vs Oil@H<sub>2</sub>O; therefore, the applied catalysts can perform denitrogenation. The alkaline-catalytic liquefaction of bio-oils produced maximum cyclic hydrocarbons (9.61 %–14.01 %) and aldehyde/ketone compounds (40.36 %–47.72 %) compared with other liquefaction bio-oils. Alcoholic (24.2 %) and carboxylic acid (10.2 %) compounds were significantly increased when H<sub>3</sub>PO<sub>4</sub> catalysts and furans were promoted using hematite catalyst. Hence, bio-oil product' chemical compositions were highly dependent on the catalyst type used in HTL. Fig. 3 (b) shows the different fractions yield and boiling point distribution of all Oil@X.

Obviously, all the obtained biocrudes exhibit large fractions in high molecular weight compounds associated with higher residual cuts of 67.10–78.10 % above 340 °C. Therefore, further upgrading processes are required to produce the fungible on-specification transportation fuel.

### 3.2. Yield, porosity, and surface chemistry of HCs and ACs

Wheat stem's physical structure shows a dense and smooth surface with few rough areas (WS SEM image, Fig. 4) because of the presence of carbohydrates that compact and make the cellulosic fibers invisible even at a high magnitude × 10000. Based on WS FTIR spectra (Fig. 5), the range of 3330.58 cm<sup>-1</sup> confirms the presence of –OH vibrations for intramolecular hydrogen bonds between cellulose chains or moisture. Two successive C–H stretching vibrations within a methyl group at 2918.01 and 2849.91 cm<sup>-1</sup> originate from stem cuticle waxes [30]. The peak at 1733.07 cm<sup>-1</sup> is associated with the carboxyl group C=O stretching vibration of acetic, uronic, p-coumaric, ferulic acids, and esters, which are the main constituents of extractives and hemicellulose [31]. The peaks at 1641.34, 1422.49, and 1367.85 cm<sup>-1</sup> were associated with lignin aromatic ring C=C stretching, C–H stretching, and C–H or O–H bending, respectively. Moreover, two characteristic lignin bands were observed near 1240.61, and 1308.48 cm<sup>-1</sup> corresponding to the C–O ring of guaiacyl and syringyl [32]. The two peaks at 1031.19 and 889.48 cm<sup>-1</sup> indicated the C–O stretching and C–H deformation vibrations of the typical absorption peak of β-glycoside linkages in lignin and cellulose, respectively. The peak at 1031.18 cm<sup>-1</sup> may also be associated with Si–O stretching [31].

After HTL under different catalysts (X) with a 2 % ratio at 350 °C for 15 min, HC surfaces show cellular networks with few mesoporous cavities, with average pore sizes of 12.79–33.58 nm, which fall between 2 and 50 nm based on the IUPAC classification (Fig. 4 and Table 2, SEM images and textural properties of HC@H<sub>2</sub>O, HC@NaOH, HC@KOH, HC@Na<sub>2</sub>CO<sub>3</sub>, HC@K<sub>2</sub>CO<sub>3</sub>, HC@H<sub>3</sub>PO<sub>4</sub>, HC@FeCl<sub>3</sub>, and HC@Fe<sub>2</sub>O<sub>3</sub>). These remarkable structural changes occurred during HTL of WS under high-pressure conditions, and the formation of mesopores (V<sub>meso</sub> = 0.018–0.068 cm<sup>3</sup>/g) with the absence of micropores (V<sub>micro</sub> = 9.10E<sup>-05</sup>–2.03E<sup>-03</sup> cm<sup>3</sup>/g) on the surface was found in all eight HCs. This can be explained by the series of reactions undergone during HTL, which softened the WS solid matrix composed of cellulose, hemicellulose, lignin, and extractives, leading to the formation of low surface

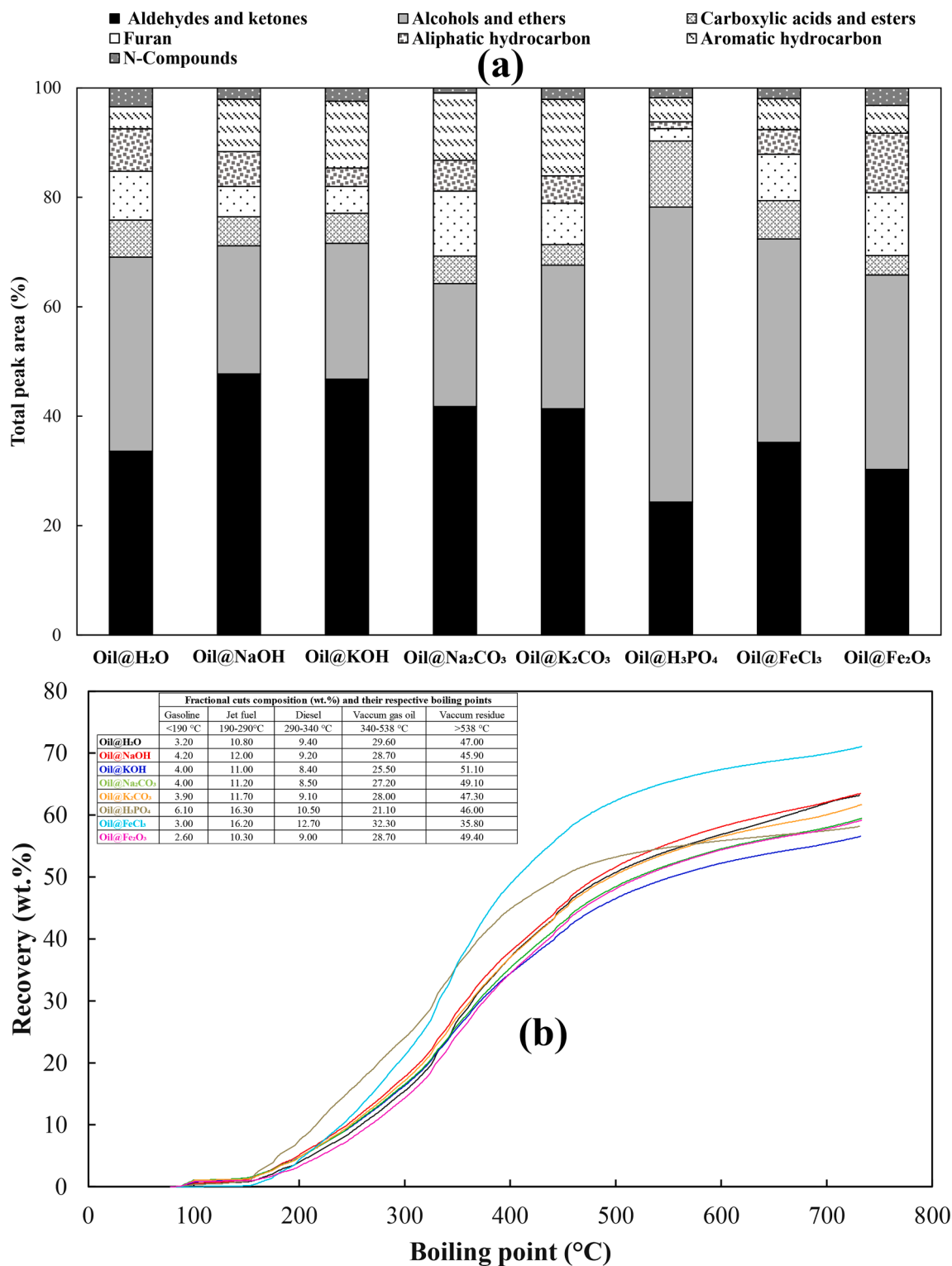


**Fig. 3.** (a) Division in groups of the organic compounds found out by GC–MS analysis of the crude bio-oils obtained at subcritical water condition for 15 min with/without catalyst, (b) Fractionation cuts composition of Oil@X at their respective boiling point.

areas of  $S_{\text{BET}} = 5.46\text{--}26.06 \text{ m}^2/\text{g}$  and total pore volumes of  $V_{\text{T}} \approx V_{\text{meso}} = 0.012\text{--}0.072 \text{ cm}^3/\text{g}$  (Table 2). Comparable liquefaction of HC surface characteristics were obtained in previous studies of de-oiled seed cakes, sewage sludge, microalgae, and rice straw [11,33,34]. Furthermore, textural features of HCs generated from alkaline-catalytic HTL had similar properties to HC@H<sub>2</sub>O, demonstrating the inclusion of NaOH, KOH, Na<sub>2</sub>CO<sub>3</sub>, and K<sub>2</sub>CO<sub>3</sub> in HTL reaction decreased HC formation,

thereby improving bio-oil production and quality. In addition, HC@H<sub>3</sub>PO<sub>4</sub>, HC@FeCl<sub>3</sub>, and HC@Fe<sub>2</sub>O<sub>3</sub> exhibited developed surfaces because of the low pH, promoting dehydration and polymerization reactions yielding HCs with  $S_{\text{BET}}$  of  $26.06 \text{ m}^2/\text{g}$ ,  $12.99 \text{ m}^2/\text{g}$ , and  $10.05 \text{ m}^2/\text{g}$ , respectively. Compared with that of WS feedstock, the FTIR spectra of HCs (Fig. 5) showed a reduction in oxygenated surface functional groups caused by dehydration reactions where the –OH stretching



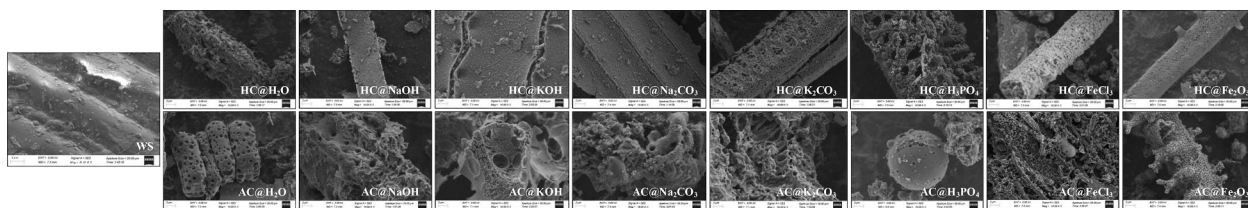


Fig. 4. SEM images at 10000 × of WS, HCs, and ACs.

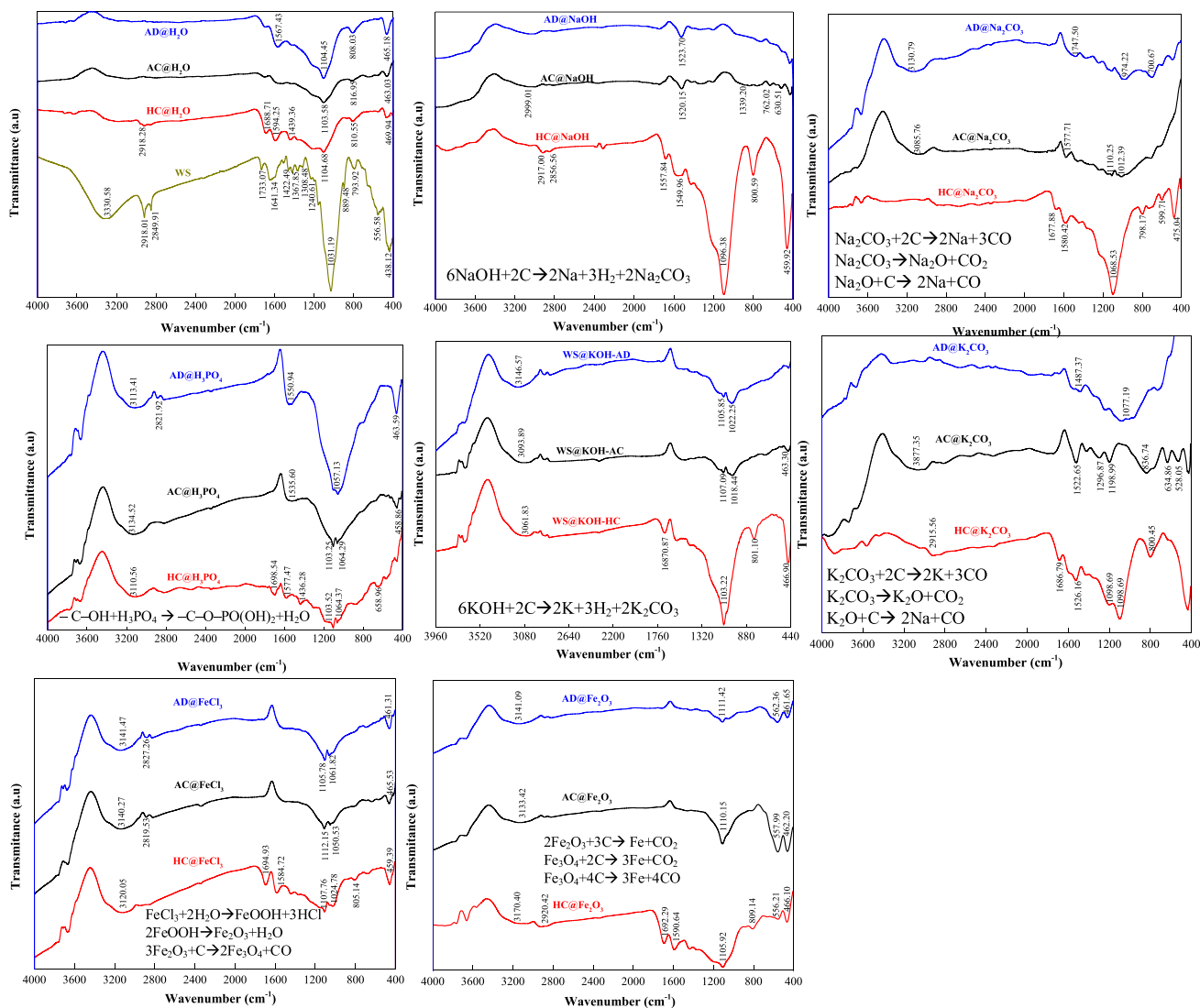


Fig. 5. FTIR spectra of WS, HCs, ACs before and after adsorption and activation mechanism.

and alkyl C—H Stretch between 3600 and 2500  $\text{cm}^{-1}$  weakened and/or disappeared, and the increase of aromatic functional groups in the presence of new peaks at 1700–1500  $\text{cm}^{-1}$  of aromatic C=C bending and 860–680  $\text{cm}^{-1}$  of aromatic C—H bonds resulted from polymerization and aromatization reactions during the formation of HC [35,36].

Activated HC SEM images (Fig. 4) showed that the chemical activation with different catalysts (X, IR = 2) at 800 °C for 90 min contributes effectively to the widening of HC mesopores to macropores and the formation of new micro- and mesopores with different sizes ( $D_p = 1.75\text{--}6.61\text{ nm}$ ) and irregular shapes ( $V_{\text{micro}} = 0.034\text{--}0.675\text{ cm}^3/\text{g}$ ,  $V_{\text{meso}} = 0.032\text{--}0.345\text{ cm}^3/\text{g}$ ) on the ACs surfaces. Hence, a sustaining increase in BET surface areas ( $S_{\text{BET}} = 100.22\text{--}1612.04\text{ m}^2/\text{g}$ ) and pore

development ( $V_T = 0.067\text{--}0.848\text{ cm}^3/\text{g}$ ) were recorded and presented in Table 2, leading to the increase in weight loss of carbon in HCs and the reduction of AC yields from 14.49 % to 38.07 % (Fig. 4 and Table 2 results of AC@H<sub>2</sub>O, AC@NaOH, AC@KOH, AC@Na<sub>2</sub>CO<sub>3</sub>, AC@K<sub>2</sub>CO<sub>3</sub>, AC@H<sub>3</sub>PO<sub>4</sub>, AC@FeCl<sub>3</sub>, and AC@Fe<sub>2</sub>O<sub>3</sub>). The enhancement of HC surface properties was obtained from the reactions between the chemical activating agents and the carbon matrix of HCs at 800 °C presented in Fig. 5 [18,37,38].

**Table 2**

Carbon yields and surface characteristics of the HCs and ACs.

Hydrochars (HCs) and activated carbons (ACs) from WS	Carbon Yield (%)	$S_{\text{BET}}$ ( $\text{m}^2/\text{g}$ )	$S_{\text{ext}}$ ( $\text{m}^2/\text{g}$ )	$S_{\text{micro}}$ ( $\text{m}^2/\text{g}$ )	$V_{\text{micro}}$ ( $\text{cm}^3/\text{g}$ )	$V_{\text{meso}}$ ( $\text{cm}^3/\text{g}$ )	$V_{\text{T}}$ ( $\text{cm}^3/\text{g}$ )	$D_p$ (nm)	
								4 V/A by BET	4 V/A by BJH
HC@H <sub>2</sub> O	33.03 ± 0.67	8.54	7.82	0.721	1.61E-04	0.025	0.012	5.58	13.77
AC@H <sub>2</sub> O	21.85 ± 0.12	253.54	62.94	190.60	0.075	0.056	0.130	2.05	6.61
HC@NaOH	22.67 ± 0.24	5.45	3.68	1.769	6.66E-04	0.028	0.029	7.14	33.58
AC@NaOH	15.20 ± 0.23	762.95	199.11	563.84	0.238	0.185	0.428	2.12	3.74
HC@KOH	22.83 ± 0.46	7.62	7.13	0.48	1.11E-04	0.032	0.032	7.93	19.16
AC@KOH	14.49 ± 0.24	1612.04	145.08	1466.96	0.675	0.345	0.848	2.06	2.84
HC@Na <sub>2</sub> CO <sub>3</sub>	22.03 ± 0.67	6.75	6.19	0.547	9.10E-05	0.023	0.023	6.18	15.42
AC@Na <sub>2</sub> CO <sub>3</sub>	16.12 ± 0.12	396.40	92.24	304.16	0.125	0.094	0.226	2.12	4.44
HC@K <sub>2</sub> CO <sub>3</sub>	25.43 ± 0.24	7.18	6.39	0.78	1.21E-04	0.018	0.019	5.58	12.79
AC@K <sub>2</sub> CO <sub>3</sub>	18.82 ± 0.46	1315.84	97.07	1218.77	0.489	0.113	0.593	1.75	3.65
HC@H <sub>3</sub> PO <sub>4</sub>	51.76 ± 0.37	26.06	23.83	2.23	7.36E-04	0.068	0.072	5.14	15.70
AC@H <sub>3</sub> PO <sub>4</sub>	38.07 ± 0.35	712.11	58.90	653.21	0.279	0.144	0.392	1.96	4.40
HC@FeCl <sub>3</sub>	35.70 ± 0.26	12.99	11.13	1.86	6.34E-04	0.039	0.041	5.93	15.60
AC@FeCl <sub>3</sub>	22.20 ± 0.26	308.69	85.46	223.22	0.089	0.132	0.219	2.626	5.17
HC@Fe <sub>2</sub> O <sub>3</sub>	36.69 ± 0.12	10.049	5.56	4.49	2.03E-03	0.023	0.024	4.099	17.00
AC@Fe <sub>2</sub> O <sub>3</sub>	22.31 ± 0.26	100.22	17.03	83.19	0.034	0.032	0.067	2.203	7.20

### 3.3. Treatment of post-HTL aqueous phase: Removal and adsorption mechanism of organics and nutrients onto activated HCs

Fig. 6(a) presents pH variation before and after treatment of the obtained aqueous phase samples (HTL-AP) at non-catalytic/catalytic HTL conditions. At the beginning of the non-catalytic HTL experiment, the slurry of the WS was at neutral pH because only water was present in the liquid phase. The pH of the resulting AP@H<sub>2</sub>O was acidic at 3.95, which was primarily due to the production of organic acids from the degradation of lignocellulosic carbohydrates during HTL [39]. These large amounts of organic matter in the liquid phase showed a TOC of 38880 mg/L, a COD of 78000 mg/L, and total phenols of 1205 mg/L. In addition, the inorganic matter in the WS was directly dissolved, which inevitably led to mineral ion' transformation into the HTL-AP as potassium (K = 2756 mg/L), phosphorous (TP = 125 mg/L), and nitrogen (TN = 277 mg/L). Moreover, the acidity of the aqueous phase intensified to 1.33 for AP@H<sub>3</sub>PO<sub>4</sub> and 3.40 for AP@FeCl<sub>3</sub>, which was related to the use of acid catalysts and the dominance of *in situ* hydroxyl radicals.

Furthermore, the pH of aqueous phase samples under alkaline catalytic HTL slightly increased up to 4.59, which indicated that some of the produced acids likely neutralized by hydroxides (NaOH, KOH) and/or carbonate salts (Na<sub>2</sub>CO<sub>3</sub>, K<sub>2</sub>CO<sub>3</sub>). After HTL-AP treatment, the pH values were in the neutral range of 6.53–8.10, related to the effect of the process prior to adsorption, in which particles suspended in HTL-AP were clumped to form larger particles by adjusting electrostatic charges using polyaluminum chloride. Polyaluminum chloride was known in the field of wastewater treatment for its effectiveness as a coagulant and its ability to neutralize settleable solids in suspension leading to the removal of organic products [40].

Fig. 6(b) and (c) show the removal percentage of organic matter (COD, TOC, and phenols) and nutrients (TN, TP, and K) from different aqueous phase samples after treatment at 30 °C with 20 g/L ratio of AC@X mass to AP@X volume. As shown in Fig. 6(b), AP@H<sub>3</sub>PO<sub>4</sub> and AP@K<sub>2</sub>CO<sub>3</sub> solutions treated by AC@H<sub>3</sub>PO<sub>4</sub> and AC@K<sub>2</sub>CO<sub>3</sub> showed the potential reduction in the content of phenols to 0.713 mg/L (99.91 %) and 2.48 mg/L (99.78 %), total organic compounds (TOC) to 1153 mg/L

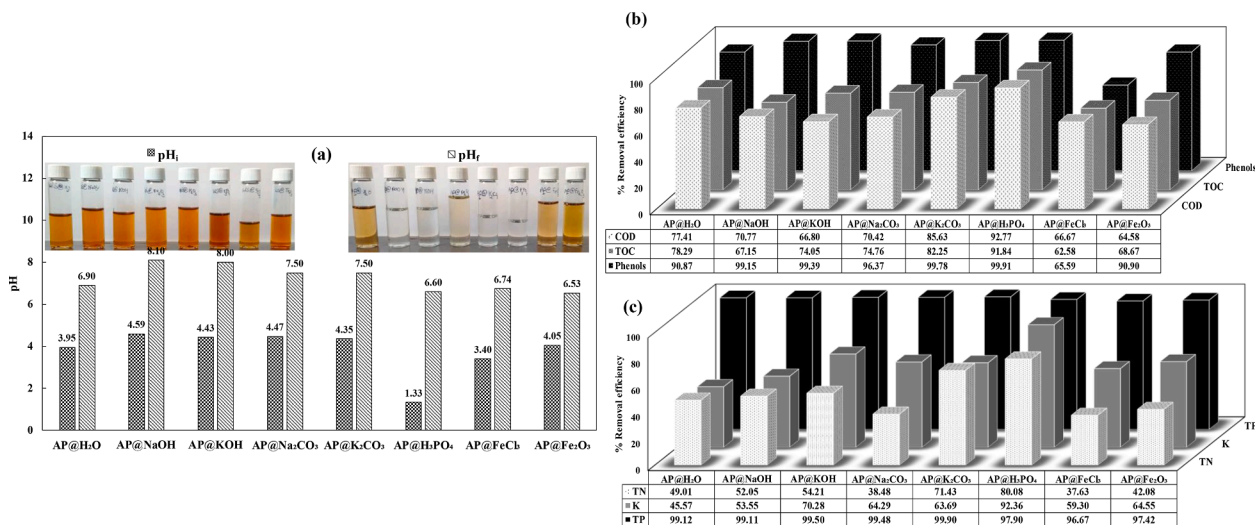


Fig. 6 (a) pH variation and HTL-AP before and after treatment (inset); (b) % Removals of COD, TOC, DOC, and phenols;

(c) % Removals of TN, TP, and total dissolved potassium (K).

**Fig. 6.** (a) pH variation and HTL-AP before and after treatment (inset); (b) % Removals of COD, TOC, DOC, and phenols; (c) % Removals of TN, TP, and total dissolved potassium (K).

(91.84 %) and 5950 mg/L (82.25 %), and oxidizable organic matter to 3340 mg/L (92.77 %) and 11380 mg/L (85.63 %), respectively. In addition, AP@Fe<sub>2</sub>O<sub>3</sub> and AP@FeCl<sub>3</sub> exhibited relatively lower TOC and COD using AC@Fe<sub>2</sub>O<sub>3</sub> and AC@FeCl<sub>3</sub>, respectively. This result may be associated with the low BET surface areas of 100.22 m<sup>2</sup>/g for AC@Fe<sub>2</sub>O<sub>3</sub> and 308.69 m<sup>2</sup>/g for AC@FeCl<sub>3</sub>, and the partial blockage of some pores with iron covering the active adsorption sites [41]. These results of organic adsorbate removals were associated not only with AC surface functional groups, but also with their adsorption capacities related to initial concentrations of adsorbates in different HTL-AP (e.g., C<sub>i,COD</sub> = 78.00 g/L in AP@ H<sub>2</sub>O, C<sub>i,COD</sub> = 79.20 g/L in AP@ K<sub>2</sub>CO<sub>3</sub>, and C<sub>i,COD</sub> = 46.20 g/L in AP@ H<sub>3</sub>PO<sub>4</sub>). Comparing the residual COD concentrations in the remaining aqueous streams (e.g., C<sub>r,COD</sub> = 17.62 g/L in AP@ H<sub>2</sub>O, C<sub>r,COD</sub> = 11.38 g/L in AP@ K<sub>2</sub>CO<sub>3</sub>, and C<sub>r,COD</sub> = 3.30 g/L in AP@ H<sub>3</sub>PO<sub>4</sub>) with the current European discharge limit [42], further optimization and/or treatment is required for disposal.

The percent removal efficiencies of nutrient adsorbates from HTL-AP are shown in Fig. 6(c), ranging from 37.63 % to 80.08 % for TN, 96.67 % to 99.89 % for TP, and 45.57 % to 92.36 % for total dissolved K. Moreover, N, P, and K elemental compositions in the activated HCs before (AC@X) and after (AD@X) adsorption were evaluated using EDX analysis. Their weight percentages with mapping images are summarized in Fig. 7, revealing their spatial distribution in the used ACs (AD@H<sub>2</sub>O, AD@NaOH, AD@KOH, AD@Na<sub>2</sub>CO<sub>3</sub>, AD@K<sub>2</sub>CO<sub>3</sub>, AD@H<sub>3</sub>PO<sub>4</sub>, AD@FeCl<sub>3</sub>, and AD@Fe<sub>2</sub>O<sub>3</sub>). These results indicate that a high phosphorous recovery up to 95 % is achieved in all treated AP@X. The phase transfer of residual P-containing compounds from HTL-AP to ACs and their uptake onto the active sites showed an increase in phosphorus content to 0.19 % in AD@H<sub>2</sub>O, 0.60 % in AD@NaOH, 0.25 % in AD@Na<sub>2</sub>CO<sub>3</sub>, 0.13 % in AD@FeCl<sub>3</sub>, and 6.22 % in AD@H<sub>3</sub>PO<sub>4</sub>. In addition, no change in %P was observed between AD@K<sub>2</sub>CO<sub>3</sub> and AD@KOH (after adsorption) and intact AC@K<sub>2</sub>CO<sub>3</sub> and AC@KOH (before adsorption). Thus, the total removal of TP can be explained not only by adsorption onto the functional groups of activated HCs but also by a remarkably fraction of TP being chemically precipitated with polyaluminium chloride. For AP@FeCl<sub>3</sub> and AP@Fe<sub>2</sub>O<sub>3</sub>, low initial concentrations of TP were found equal to 30 mg/L < 125 mg/L (in AP@H<sub>2</sub>O), indicating that FeCl<sub>3</sub> and Fe<sub>2</sub>O<sub>3</sub> catalysts enhanced the precipitation of P in the form of iron phosphate and its accumulation in the solid residue during HTL reaction. Consequently, slight adsorption rates

of the residual P from 0.09 to 0.13 % in AD@FeCl<sub>3</sub> and from 0.01 % to 0.04 % in AD@Fe<sub>2</sub>O<sub>3</sub> were shown. The removal of TN and dissolved potassium (K) was nearly 60 % with high values of 80.08 % and 92.36 % for AP@H<sub>3</sub>PO<sub>4</sub>, respectively. The uptake of N-containing compounds was examined in all adsorptions runs, and the strongest distribution of green dots was found in the spots of AD@Fe<sub>2</sub>O<sub>3</sub>, followed by chemically activated alkaline-based carbons, AD@H<sub>2</sub>O, AD@FeCl<sub>3</sub>, and AD@H<sub>3</sub>PO<sub>4</sub>. This order was consistent with the relative weight percentages presented in Fig. 7. A similar trend was observed by studying the distribution of blue color in adsorbed K onto the active sites of ACs over the entire images in the following order: AD@FeCl<sub>3</sub> > AD@H<sub>2</sub>O > AD@K<sub>2</sub>CO<sub>3</sub> > AD@KOH > AD@NaOH > AD@Na<sub>2</sub>CO<sub>3</sub> > AD@H<sub>3</sub>PO<sub>4</sub>. The prepared activated HCs demonstrate affinity to nutrients (N, P, and K) and their recovery from the aqueous phase and loading into ACs, which can be attributed to complexation, including hydrogen bonding and electrostatic attraction [43–45].

The comparison between the FTIR spectra of the AC@X with the corresponding AD@X can illustrate the possible mechanism of organics and nutrient adsorption onto activated HCs. Analysis revealed that the shifting and disappearance of 3100 cm<sup>-1</sup>, 15567 cm<sup>-1</sup>, 1339.20 cm<sup>-1</sup>, 1296 cm<sup>-1</sup> and 836 cm<sup>-1</sup> peaks, indicating their role in adsorption. Furthermore, shifting in aromatic C=C from 1522 to 1487 cm<sup>-1</sup>, such a change in chemical structure, suggests the potential  $\pi$ - $\pi$  stacking between the aromatic ring of ACs and organic adsorbates in HTL-AP. Similar mechanisms have been reported for the uptake of 91.84 % COD, 80.0 % phenols, 91.08 % nitrogen, and 99.98 % phosphate onto pyrolytic bamboo-based activated carbon [46], rice-husk activated carbon [47], modified zeolite-diatomite composite [48], La-wheat straw biochar [44], respectively.

#### 4. Conclusion

The current study revealed that HTL at subcritical water conditions followed by HTL-AP treatment using the twofold K<sub>2</sub>CO<sub>3</sub> role as a homogeneous catalyst and an activating agent is the most combinatorial scheme in terms of HTL products yield and quality. This resulted in yielding 28.79 % biocrude, 34.36 MJ/kg HHV, 59.27 % energy recovery, 18.82 % activated HC with S<sub>BET</sub> = 1315.84 m<sup>2</sup>/g, and the uptake and recovery of 82.25 % of organic adsorbates (TOC), 71.43 % of total nitrogen. The analysis of gas chromatography GC/MS, simulated-

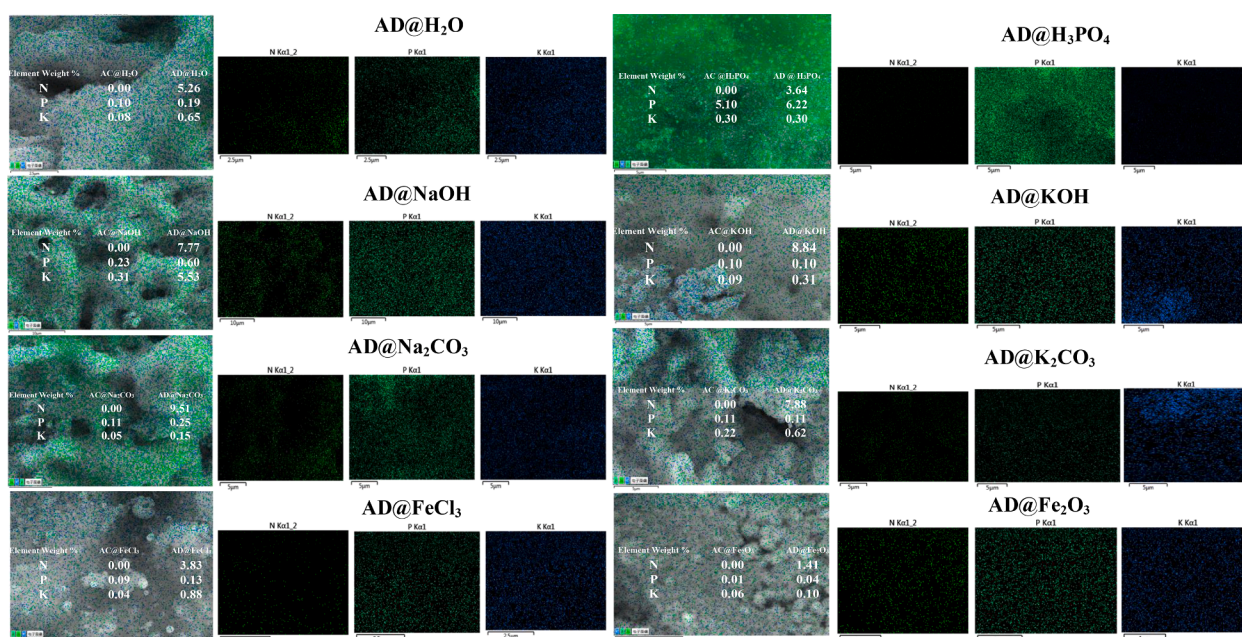


Fig. 7. Weight percentages of N, P and K before (AC@X) and after adsorption (AD@X) with EDX mapping images.



distillation, and elemental (CHNO) composition revealed that biocrude has high oxygenated compounds, suggesting that upgrading is required for drop-in transportation-grade fuel. The feasibility of removing organics and nutrients from HTL-AP and their recovery onto the carbon matrix of the hydrochar has been elucidated in this research, proving that design and modeling adsorption parameters (e.g., pH, temperature, time, etc.) can be discovered. Conducting a Techno-Economic Analysis of HTL integrated with the activation of hydrochar to a carbon adsorbent and its application for the HTL-AP post-treatment can be as well explored towards a scalable and circular implementation.

### CRedit authorship contribution statement

**Fatma Marrakchi:** Conceptualization, Investigation, Methodology, Supervision, Validation, Data curation, Visualization, Writing – original draft, Writing – review & editing. **Saqib Sohail Toor:** Resources (Technical support for autoclave reactor), Validation. **Asbjørn Haaning Nielsen:** Investigation (ICP Analysis). **Thomas Helmer Pedersen:** Validation. **Lasse Aistrup Rosendahl:** Validation.

### Declaration of Competing Interest

The authors declare that they have no known competing financial interests or personal relationships that could have appeared to influence the work reported in this paper.

### Data availability

Data will be made available on request.

### Acknowledgment

CO-HTL4BIO-OIL project has received funding from the European Union's Horizon 2020 research and innovation programme under the Marie Skłodowska-Curie grant agreement ID 895710 (<https://cordis.europa.eu/project/id/895710>).

### References

- [1] P. D'Odorico, J. Dell'Angelo, N. Galli, L.A.H. Nogueira, T. Richard, M. Santini, Roadmap to 2050: The Land-Water-Energy Nexus of Biofuels, (2021).
- [2] P. Sundarajan, K.P. Gopinath, J. Arun, K. GracePavithra, A. Adithya Joseph, S. Manasa, Insights into valuing the aqueous phase derived from hydrothermal liquefaction, *Renew. Sustain. Energy Rev.* 144 (2021), 111019.
- [3] L. Leng, W. Zhang, H. Peng, H. Li, S. Jiang, H. Huang, Nitrogen in bio-oil produced from hydrothermal liquefaction of biomass: a review, *Chem. Eng. J.* 401 (2020), 126030.
- [4] A.R.K. Gollakota, N. Kishore, S. Gu, A review on hydrothermal liquefaction of biomass, *Renew. Sustain. Energy Rev.* 81 (2018) 1378–1392.
- [5] J. Watson, T. Wang, B. Si, W.-T. Chen, A. Aierzhati, Y. Zhang, Valorization of hydrothermal liquefaction aqueous phase: pathways towards commercial viability, *Prog. Energy Combust. Sci.* 77 (2020) 100819.
- [6] A. Swetha, S. Shrivigneshwar, K.P. Gopinath, R. Sivaramkrishnan, R. Shanmuganathan, J. Arun, Review on hydrothermal liquefaction aqueous phase as a valuable resource for biofuels, bio-hydrogen and valuable bio-chemicals recovery, *Chemosphere* 283 (2021), 131248.
- [7] M. Tsarpali, N. Arora, J.N. Kuhn, G.P. Philippidis, Beneficial use of the aqueous phase generated during hydrothermal carbonization of algae as nutrient source for algae cultivation, *Algal Res.* 60 (2021), 102485.
- [8] R. Li, D. Liu, Y. Zhang, G. Tommaso, B. Si, Z. Liu, N. Duan, Enhanced anaerobic digestion of post-hydrothermal liquefaction wastewater: Bio-methane production, carbon distribution and microbial metabolism, *Sci. Total Environ.* 837 (2022), 155659.
- [9] F. Marrakchi, F. Fazeli Zafar, M. Wei, C. Yuan, B. Cao, S. Wang, N-doped mesoporous  $H_3PO_4$ -pyrocarbon from seaweed and melamine for batch adsorption of the endocrine disruptor bisphenol A, *Journal of Molecular Liquids*. 345 (2022) 117040.
- [10] S. Masoumi, A.K. Dalai, Optimized production and characterization of highly porous activated carbon from algal-derived hydrochar, *J. Cleaner Prod.* 263 (2020), 121427.
- [11] V.K. Ponnusamy, S. Nagappan, R.R. Bhosale, C.-H. Lay, D. Duc Nguyen, A. Pugazhendhi, S.W. Chang, G. Kumar, Review on sustainable production of biochar through hydrothermal liquefaction: Physico-chemical properties and applications, *Bioresour. Technol.* 310 (2020), 123414.
- [12] L. Björnsson, T. Prade, Sustainable cereal straw management: use as feedstock for emerging biobased industries or cropland soil incorporation? *Waste Biomass Valor.* 12 (2021) 5649–5663.
- [13] ASTM D482-19, Standard Test Method for Ash from Petroleum Products, (2019).
- [14] T.H. Seehar, S.S. Toor, A.A. Shah, T.H. Pedersen, L.A. Rosendahl, Biocrude production from wheat straw at sub and supercritical hydrothermal liquefaction, *Energies* 13 (2020) 3114.
- [15] Z. Zhu, S.S. Toor, L. Rosendahl, D. Yu, G. Chen, Influence of alkali catalyst on product yield and properties via hydrothermal liquefaction of barley straw, *Energy* 80 (2015) 284–292.
- [16] K. Kohansal, S. Toor, K. Sharma, R. Chand, L. Rosendahl, T.H. Pedersen, Hydrothermal liquefaction of pre-treated municipal solid waste (biopulp) with recirculation of concentrated aqueous phase, *Biomass Bioenergy* 148 (2021), 106032.
- [17] ASTM D7169-20, Standard Test Method for Boiling Point Distribution of Samples with Residues Such as Crude Oils and Atmospheric and Vacuum Residues by High Temperature Gas Chromatography, (2020).
- [18] F. Marrakchi, F. Fazeli Zafar, M. Wei, S. Wang, Cross-linked  $FeCl_3$ -activated seaweed carbon/MCM-41/alginate hydrogel composite for effective biosorption of bisphenol A plasticizer and basic dye from aqueous solution, *Bioresour. Technol.* 331 (2021) 125046.
- [19] M. Wei, F. Marrakchi, C. Yuan, X. Cheng, D. Jiang, F.F. Zafar, Y. Fu, S. Wang, Adsorption modeling, thermodynamics, and DFT simulation of tetracycline onto mesoporous and high-surface-area NaOH-activated macroalgae carbon, *J. Hazard. Mater.* 425 (2022), 127887.
- [20] F. Marrakchi, M. Bouaziz, B.H. Hameed, Activated carbon-clay composite as an effective adsorbent from the spent bleaching sorbent of olive pomace oil: Process optimization and adsorption of acid blue 29 and methylene blue, *Chem. Eng. Res. Des.* 128 (2017) 221–230.
- [21] S.S. Toor, L. Rosendahl, A. Rudolf, Hydrothermal liquefaction of biomass: a review of subcritical water technologies, *Energy* 36 (2011) 2328–2342.
- [22] B. Zhao, H. Li, H. Wang, Y. Hu, J. Gao, G. Zhao, M.B. Ray, C.C. Xu, Synergistic effects of metallic Fe and other homogeneous/heterogeneous catalysts in hydrothermal liquefaction of woody biomass, *Renew. Energy* 176 (2021) 543–554.
- [23] J. Akhtar, S.K. Kuang, N.S. Amin, Liquefaction of empty palm fruit bunch (EPFB) in alkaline hot compressed water, *Renew. Energy* 35 (6) (2010) 1220–1227.
- [24] S. Zhou, D. Mourant, C. Lievens, Y. Wang, C.-Z. Li, M. Garcia-Perez, Effect of sulfuric acid concentration on the yield and properties of the bio-oils obtained from the auger and fast pyrolysis of Douglas Fir, *Fuel* 104 (2013) 536–546.
- [25] E.M. Chatir, A. El Hadrami, S. Ojala, R. Brahmi, Production of activated carbon with tunable porosity and surface chemistry via chemical activation of hydrochar with phosphoric acid under oxidizing atmosphere, *Surf. Interfaces* 30 (2022), 101849.
- [26] M. Jagtoyen, F. Derbyshire, Activated carbons from yellow poplar and white oak by  $H_3PO_4$  activation, *Carbon* 36 (7–8) (1998) 1085–1097.
- [27] B. de Caprariis, I. Bavasso, M.P. Bracciale, M. Damizia, P. De Filippis, M. Scarsella, Enhanced bio-crude yield and quality by reductive hydrothermal liquefaction of oak wood biomass: effect of iron addition, *J. Anal. Appl. Pyrol.* 139 (2019) 123–130.
- [28] D. Castello, M.S. Haider, L.A. Rosendahl, Catalytic upgrading of hydrothermal liquefaction biocrudes: Different challenges for different feedstocks, *Renewable Energy* 141 (2019) 420–430.
- [29] F. Conti, S.S. Toor, T.H. Pedersen, T.H. Seehar, A.H. Nielsen, L.A. Rosendahl, Valorization of animal and human wastes through hydrothermal liquefaction for biocrude production and simultaneous recovery of nutrients, *Energy Convers. Manage.* 216 (2020), 112925.
- [30] W. Stelte, C. Clemons, J.K. Holm, J. Ahrenfeldt, U.B. Henriksen, A.R. Sanadi, Fuel pellets from wheat straw: the effect of lignin glass transition and surface waxes on pelletizing properties, *Bioenerg. Res.* 5 (2012) 450–458.
- [31] M. Sain, S. Panthapulakkal, Bioprocess preparation of wheat straw fibers and their characterization, *Ind. Crops Prod.* 23 (1) (2006) 1–8.
- [32] Y. Deng, Y. Qiu, Y. Yao, M. Ajania, M. Davaritouchee, Weak-base pretreatment to increase biomethane production from wheat straw, *Environ Sci Pollut Res.* 27 (30) (2020) 37989–38003.
- [33] D. Kumar, K.K. Pant, Production and characterization of biocrude and biochar obtained from non-edible de-oiled seed cakes hydrothermal conversion, *J. Anal. Appl. Pyrol.* 115 (2015) 77–86.
- [34] L. Leng, X. Yuan, H. Huang, H. Wang, Z. Wu, L. Fu, X. Peng, X. Chen, G. Zeng, Characterization and application of bio-chars from liquefaction of microalgae, lignocellulosic biomass and sewage sludge, *Fuel Process. Technol.* 129 (2015) 8–14.
- [35] H. Liu, I.A. Basar, A. Nzihou, C. Eskicioglu, Hydrochar derived from municipal sludge through hydrothermal processing: a critical review on its formation, characterization, and valorization, *Water Res.* 199 (2021), 117186.
- [36] N. Saha, K. McGaughey, M.T. Reza, Elucidating hydrochar morphology and oxygen functionality change with hydrothermal treatment temperature ranging from subcritical to supercritical conditions, *J. Anal. Appl. Pyrol.* 152 (2020), 104965.
- [37] K.Y. Foo, B.H. Hameed, Coconut husk derived activated carbon via microwave induced activation: Effects of activation agents, preparation parameters and adsorption performance, *Chem. Eng. J.* 184 (2012) 57–65.
- [38] F. Marrakchi, M.J. Ahmed, W.A. Khanday, M. Asif, B.H. Hameed, Mesoporous-activated carbon prepared from chitosan flakes via single-step sodium hydroxide activation for the adsorption of methylene blue, *Int. J. Biol. Macromol.* 98 (2017) 233–239.
- [39] R.B. Carpio, C.I.L. Avendaño, C.A. Basbas, A.A. Habulan, G.A.M. Guerrero, M. C. Maguyon-Detras, M.E. Bambase, Assessing the effect of  $K_2CO_3$  and aqueous

- phase recycling on hydrothermal liquefaction of corn stover, *Bioresour. Technol. Rep.* 18 (2022), 101093.
- [40] J. Greenwood, How are coagulants and flocculants used in water and wastewater treatment?, (2022).
- [41] S.-K. Ahn, K.-Y. Park, W. Song, Y. Park, J.-H. Kweon, Adsorption mechanisms on perfluorooctanoic acid by FeCl<sub>3</sub> modified granular activated carbon in aqueous solutions, *Chemosphere* 303 (2022), 134965.
- [42] E.U. Directive, Council Directive of 21 May 1991 concerning urban waste water treatment, *Regulation (EC)*. 50 (2003) 1.
- [43] X. Li, J. Shi, Simultaneous adsorption of tetracycline, ammonium and phosphate from wastewater by iron and nitrogen modified biochar: Kinetics, isotherm, thermodynamic and mechanism, *Chemosphere* 293 (2022), 133574.
- [44] Y. Huang, X. Lee, M. Grattieri, M. Yuan, R. Cai, F.C. Macazo, S.D. Minter, Modified biochar for phosphate adsorption in environmentally relevant conditions, *Chem. Eng. J.* 380 (2020), 122375.
- [45] I.W. Almanassra, G. McKay, V. Kochkodan, M. Ali Atieh, T. Al-Ansari, A state of the art review on phosphate removal from water by biochars, *Chem. Eng. J.* 409 (2021), 128211.
- [46] A.A. Ahmad, B.H. Hameed, Reduction of COD and color of dyeing effluent from a cotton textile mill by adsorption onto bamboo-based activated carbon, *J. Hazard. Mater.* 172 (2-3) (2009) 1538–1543.
- [47] Y. Fu, Y. Shen, Z. Zhang, X. Ge, M. Chen, Activated bio-chars derived from rice husk via one- and two-step KOH-catalyzed pyrolysis for phenol adsorption, *Sci. Total Environ.* 646 (2019) 1567–1577.
- [48] B. Zhang, X. Wang, S. Li, Y. Liu, Y. An, X. Zheng, Preferable adsorption of nitrogen and phosphorus from agricultural wastewater using thermally modified zeolite-diatomite composite adsorbent, *Water* 11 (2019) 2053.